Optics Communications 474 (2020) 126185

Contents lists available at ScienceDirect

Optics Communications

journal homepage: www.elsevier.com/locate/optcom

Optical properties of two dimensional fractal shaped nanostructures: Comparison of Sierpinski triangles and Sierpinski carpets

Abdolreza Rasouli Kenari [a], M. Solaimani [b,*]

[a] Faculty of Electrical and Computer Engineering, Qom University of Technology, Qom, Iran
[b] Department of Physics, Faculty of Science, Qom University of Technology, Qom, Iran

ARTICLE INFO

Keywords:
$GaAs/Al_xGa_{1-x}As$
Optical absorption coefficients
Electronic properties
Sierpinski triangles
Sierpinski carpets

ABSTRACT

In the current study, for the first time, we numerically investigate the optical properties of fixed surface area Sierpinski triangles and Sierpinski carpets. We solve the two dimensional Schrödinger equation by using three-point centered difference method in the Cartesian coordinate. By using the proposed Sierpinski systems, wave function engineering is now possible. We illustrate the wave function symmetry breaking and symmetry conservation in the Sierpinski triangle and carpet confining potentials. We have also evaluated the tunability of the optical properties of the studied systems and determined the more tunable one. We showed that the behavior of the absorption coefficient is completely different in the Sierpinski carpets and triangles. We compared two different system shapes of the case I (antidot) and case II (dot) systems and discussed the differences in their optical properties.

1. Introduction

Zero-dimensional quantum systems (quantum dots) can confine carriers in all three spatial dimensions. Due to this confinement effect, similar to atoms, electrons in quantum dots will have discretized energy levels. Therefore, quantum dots have usually been called artificial atoms. Quantum dots have a size-dependent broad excitation and a narrow emission spectrum. They also allow efficient multicolor imaging of biological systems [1] and have potential application in different optoelectronic devices such as optical amplifiers [2], infrared photodetectors [3], photodiodes [4], lasers [5], solar cells [6], photonic-crystal waveguides [7], etc. To devise such devices, studying the optical properties of the quantum dote is a necessary task.

Different optical properties of quantum dots such as optical susceptibility [8], optical rectification [9], photoluminescence [10], oscillator strength [11], optical transitions [12], the second [13] and third-harmonic generation [14], miniband formation [15], etc. have so far been studied. Among the optical properties of the quantum dot nanostructures, the absorption coefficient has a special situation. So far effects of the laser radiation [16], donor impurity [17], an exciton [18], electric and magnetic fields [19], Rashba spin–orbit interaction [20], two electrons [21], three electrons [22], electron–phonon interaction [23], temperature and hydrostatic pressure [24], interdiffusion [25], etc. on the absorption coefficient of quantum dots have been investigated. Along with these effects, effects of different shape of the quantum dot and type of the confining potential such as parabolic quantum dots [26], Gaussian potentials [27], generalized Hulthén potential [28], modified Poschl–Teller potential [29], disk-like quantum dots [30], capping layer in spherical layer quantum dots [31], core–shell nanodots [32], etc. on the absorption coefficient of quantum dots have extensively been explored.

Besides, in the theoretical and computational investigations of quantum dot optical properties, different methods such as finite-element [33], exact diagonalization [34], Quantum Genetic Algorithm [35], quantum Monte Carlo [36], nonequilibrium Green-function [37], finite difference method [38], etc. have so far been employed.

Experimental discovery of quasicrystals had a great influence on solid-state physics development [39]. Quasicrystals are an intermediate state between random media and periodic crystals. Fractal structures such as Fractal Cantor [40], Fibonacci [41], and Thue–Morse [42], etc. are aperiodic (or quasiperiodic) systems that are among the vastly studied quasicrystals. Due to the unique geometry of these systems, the energy spectrum of them can exhibit a self-similar structure [43,44]. However, the nature of a state is mathematically determined by evaluating the spectrum to which it belongs. These systems can also have other outstanding properties such as Anderson localization [45], singular continuous spectra [46], etc. Also, optical properties of Cantor-like superlattices [44], optical harmonic generation of Fibonacci dielectric Superlattices [47], and optical rectification coefficients of Fibonacci ordered multiple quantum well systems [48], the thermal conductivity of Fibonacci quasicrystals [49], as well as electronic energy spectra of two dimensional Penrose lattices [50], splitting rules for spectra

* Corresponding author.
E-mail address: solaimani@qut.ac.ir (M. Solaimani).

https://doi.org/10.1016/j.optcom.2020.126185
Received 2 April 2020; Received in revised form 30 May 2020; Accepted 9 June 2020
Available online 12 June 2020

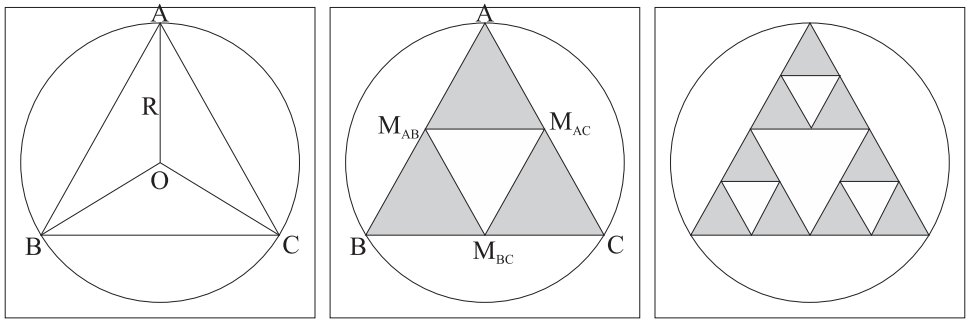

Fig. X. (a) The base △(ABC) with center O and radius R. (b) The middle points of the sides. (c) The second iteration of Sierpinski Triangles.

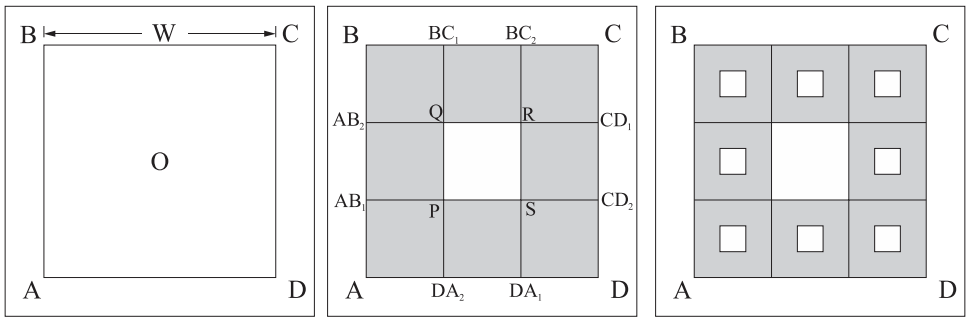

Fig. XX. (a) The base □(ABCD) with center O and width W. (b) The 1/3 and 2/3 points of the sides. (c) The second iteration of Sierpinski Carpet.

of two-dimensional Fibonacci quasilattices [51], etc. have also been considered. Among other fractal shaped structures, Sierpinski ones have less been studied. Electronic transport properties [52,53], phonon states [54], Hall conductivity [55], the spectrum of the Schrödinger equation [56], the density of states [57], etc. of Sierpinski lattices have so far been studied. But, up to our knowledge, the absorption coefficients of the fixed surface area quantum dots with the Sierpinski triangle and carpets have not so far been studied. In this work, we have studied the optical absorption of the Sierpinski triangle and Sierpinski carpets shaped semiconducting nano-systems. This is a great development of the simpler triangular [58] and square [59] quantum dot systems. Here, we have solved the resulting two dimensional Schrödinger equation by using a finite difference method. Then, we have evaluated the absorption coefficient in the compact density matrix formalism.

2. Formalism

Physical properties of an electron in a two-dimensional quantum system in the envelope function approximation and effective mass formalism can be interpreted by a Schrödinger equation,

$$H\psi(x,y) = \left[\frac{\hat{P}^2}{2m^*} + V(x,y)\right]\psi(x,y) = E\psi(x,y) \tag{1}$$

where m* and $\hat{P} = i\hbar\overrightarrow{\nabla}$ are the effective mass and momentum operator, respectively.

$$V(x,y) = \begin{cases} 1 & \text{if (x, y) inside Sierpinski Triangles or Carpet} \\ 0 & \text{else} \end{cases} \tag{2}$$

According to Refs. [60,61] suppose that we have a zone with a size of L × L. The Sierpinski fractal set is defined by the δ function and could be computed recursively by below equation.

$$L_n(x,y) = L_{n-1}(x,y) \otimes m_n(x,y) \tag{3a}$$

$$m_n(x,y) = \sum_{i=1}^{FD} \delta(x - x_i/DV^n, y - y_i/DV^n) \tag{3b}$$

where $m_n(x, y)$ is the iteration function of the fractal, n is the number of iterations, FD is the number of shapes derived from the last step (for example in Sierpinski triangles $FD = 3$, because each triangle divides to 3 triangles and in Sierpinski carpet $FD = 8$ because each rectangle divides to 8 rectangles), and DV is the number of division for each edge (for example in Sierpinski triangles $DV = 2$, because each triangle edge divides to 2 segments and in Sierpinski carpet $DV = 3$ because each rectangle edge divides to 3 segments). Finally, $L_n(x, y)$ can be rewritten as

$$\begin{aligned} &L_n(x,y) = L_0(x,y) \otimes m_1(x,y) \otimes m_2(x,y) \otimes \cdots \otimes m_n(x,y) \\ &where\ L_0(x,y) = \delta(x,y) \end{aligned} \tag{4}$$

Based on the above definition two recursive algorithms are designed to find the Sierpinski Triangles Set and Carpet Set, L_n^T, and L_n^C, respectively.

$$L_n^T = \{\triangle_{ij}(ABC) \,|\, i = 1, 2, \ldots, n \text{ and } j = 3^0, 3^1, \ldots, 3^n\} \tag{5a}$$

$$L_n^C = \{\square_{ij}(ABCD) \,|\, i = 1, 2, \ldots, n \text{ and } j = 8^0, 8^1, \ldots, 8^n\} \tag{5b}$$

To control the size of the base triangle in $L_0(x, y)$, we defined a new parameter R as the radius of the inscribed circle of the based triangle.

To build the L_n^T we have used the following procedure as depicted in Fig. X

1. Define an empty set L_0^T.
2. Find the center of the rectangular surface as O.
3. Draw a circle with center O and the specified radius R.
4. Find the three vertices of the equilateral triangle △(ABC).
5. Add △(ABC) to L_0^T.
6. Compute the middle points of $\overline{AB}$, $\overline{AC}$, $\overline{BC}$ as M_{AB}, M_{AC}, and M_{BC} (remember that the DV = 2).
7. Add △($AM_{AB}M_{AC}$)), △($BM_{AB}M_{BC}$)), △($CM_{AC}M_{BC}$)) to m_i.

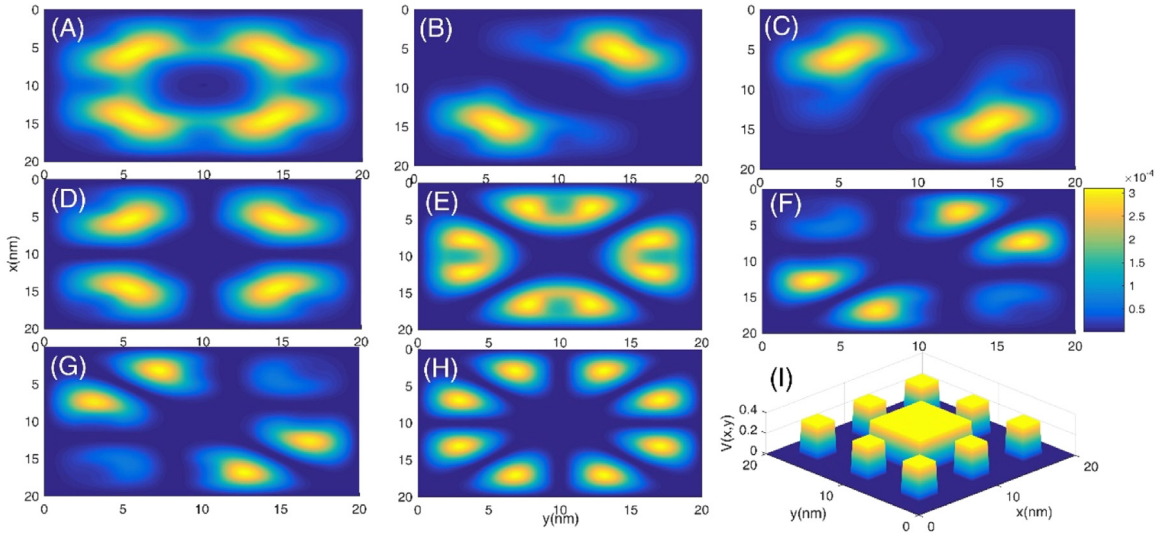

Fig. 1a. The probability densities of eight lowest eigenstates of a Sierpinski carpet of type (I) with iteration level 2 as a function of the positions x (nm) and y (nm). Panel (I): Variation of the Sierpinski carpet confining potential V(x, y) (eV) as a function of the x (nm) and y (nm).

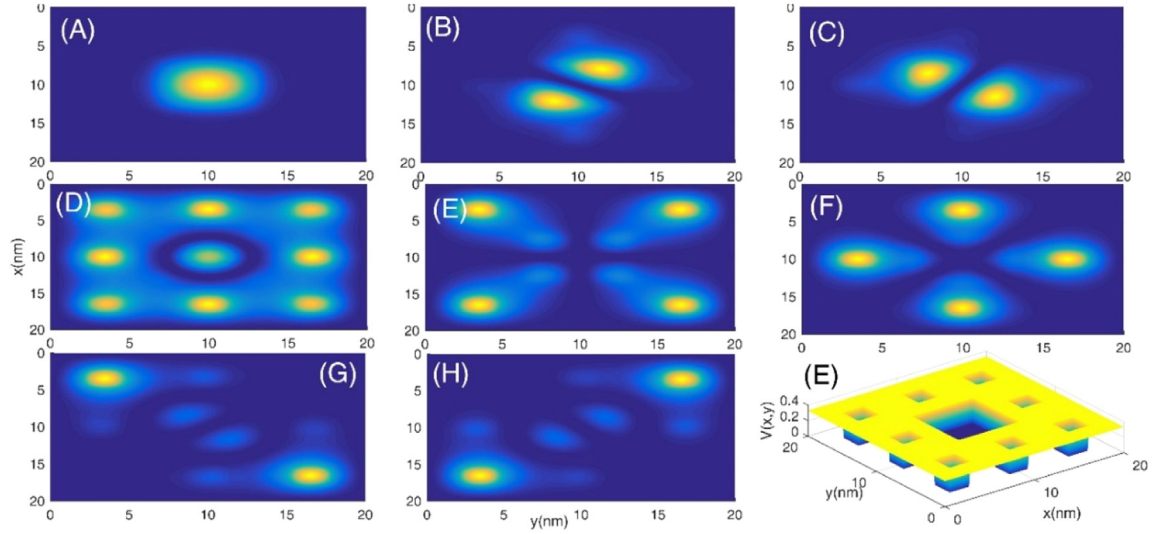

Fig. 1b. Same as Fig. 1a but for case (II) confining potential.

8. $L_i^T = L_{i-1}^T \otimes m_i$.
9. Repeat steps 6 and 7 for FD=3 new triangles $\triangle(AM_{AB}M_{AC})$, $\triangle(BM_{AB}M_{BC})$, $\triangle(CM_{AC}M_{BC})$ until L_n^T is reached.

Also, to build the Sierpinski carpet set L_n^C, the following procedure is used as depicted in Fig. XX. Again to control the size of the base rectangle in $L_0(x, y)$, we defined a new parameter W.

1. Define an empty set L_0^C.
2. Find the center of the rectangular surface as O.
3. Find the four vertices of the square with center O and the specified width W as □(ABCD).
4. Add □(ABCD) to L_0^C.
5. Divide each side $\overline{AB}$, $\overline{BC}$, $\overline{CD}$, $\overline{DA}$ into three parts (remember that the DV = 3) and find the points AB_1, AB_2, BC_1, BC_2, CD_1, CD_2, DA_1, and DA_2.
6. Divide each side $\overline{AB_1CD_2}$ into three parts and find the points P and S.
7. Divide each side $\overline{AB_2CD_1}$ into three parts and find the points Q and R.
8. Add □(A_AB_1_P_DA_2), □(AB_1_AB_2_Q_P), □(AB_2_B_BC_1_Q), □(Q_BC_1_BC_2_R), □(R_BC_2_C_CD_1), □(S_R_CD_1_CD_2), □(DA_1_S_CD_2_D), □(DA_2_P_S_DA_1) to m_i.
9. $L_i^C = L_{i-1}^C \otimes m_i$.
10. Repeat steps 5 to 8 for FD=8 new above squares until L_n^C is reached.

In the finite difference scheme to solve Eq. (1), we approximate the second derivatives by,

$$\left(\frac{d^2 f}{dx^2}\right)_{x=x_n} \approx \frac{f(x+h) - 2f(x) + f(x-h)}{h^2} \tag{6}$$

Where, $h = \frac{x_k - x_0}{N+1}$ with $x_k = x0 + k_h$ and k = 1, 2, …, N + 1. Now, try to convert it to a matrix form. If N_x and N_y are the number of discretization point along x and y axes,

$$H\psi(x,y) = -\frac{\hbar^2}{2m^*}\frac{\psi(x+\Delta x,y) - 2\psi(x,y) + \psi(x-\Delta x,y)}{\Delta x^2} - \frac{\hbar^2}{2m^*}\frac{\psi(x,y+\Delta y) - 2\psi(x,y) + \psi(x,y-\Delta y)}{\Delta y^2} + V(x,y)\psi(x,y) \tag{7}$$

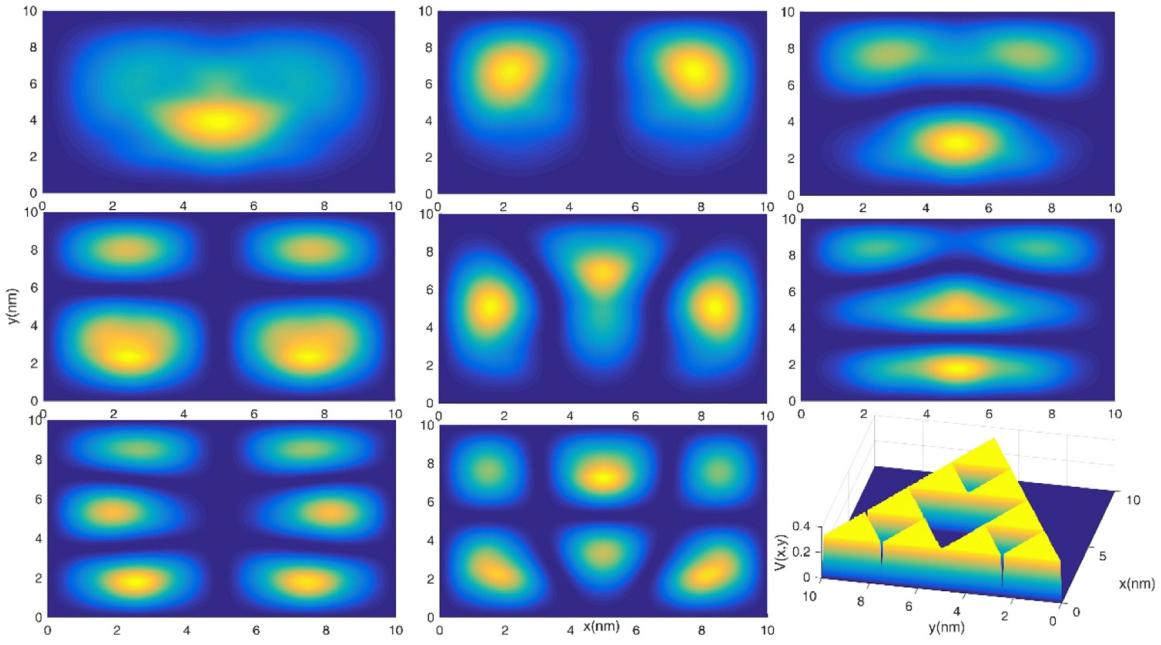

Fig. 1c. Same as Fig. 1a but for a few Sierpinski triangles.

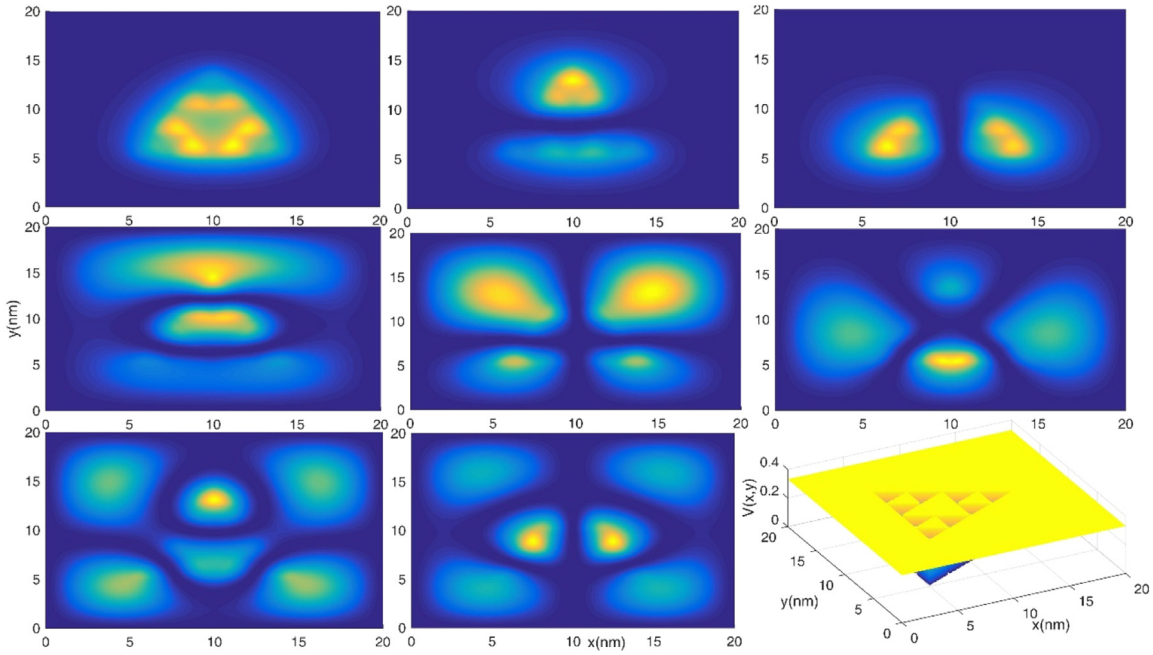

Fig. 1d. Same as Fig. 1b but for a few Sierpinski triangles.

Then,

$$H^{n,m} = -\frac{\hbar^2}{2m^*}\frac{\psi_{n+1,m} - 2\psi_{n,m} + \psi_{n-1,m}}{\Delta x^2} - \frac{\hbar^2}{2m^*}\frac{\psi_{n,m+1} - 2\psi_{n,m} + \psi_{n,m-1}}{\Delta y^2} + V(n,m)\psi_{n,m} \tag{8}$$

Now, H is a (Nx×Ny)×(Nx×Ny) matrix and $\psi_{n,m}$ is also a Nx×Ny-element vector. Therefore, we have the following matrix eigenvalue problem,

$$\left[\hat{H} - E\right]_{(\mathrm{Nx}\times\mathrm{Ny})\times(\mathrm{Nx}\times\mathrm{Ny})} [\psi]_{1\times(\mathrm{Nx}\times\mathrm{Ny})} = 0 \tag{9}$$

After diagonalization, we evaluate the linear absorption coefficient for $(E_{\mathrm{f}} - E_{\mathrm{i}})$ transition in the compact density matrix formalism as [62,63],

$$\alpha^{(1)}(\omega) = \omega\sqrt{\frac{\mu}{\varepsilon_r}} \times \frac{\sigma_s e^2 \left|M_{fi}\right|^2 \hbar\Gamma_{fi}}{(\hbar\omega - \Delta E_{fi})^2 + (\hbar\Gamma_{fi})^2} \tag{10}$$

where ω is the frequency of the excitation electromagnetic field. σ_s represents electron density in this system, E_i and E_f denote the quantized energy levels for the initial and final states, respectively, μ is the permeability, and $\Gamma_{fi}\,(f \neq i)$ is the inverse of relaxation time T_{fi} for states $|f\rangle$ and $|i\rangle$, namely $\Gamma_{fi} = 1/T_{fi}$.

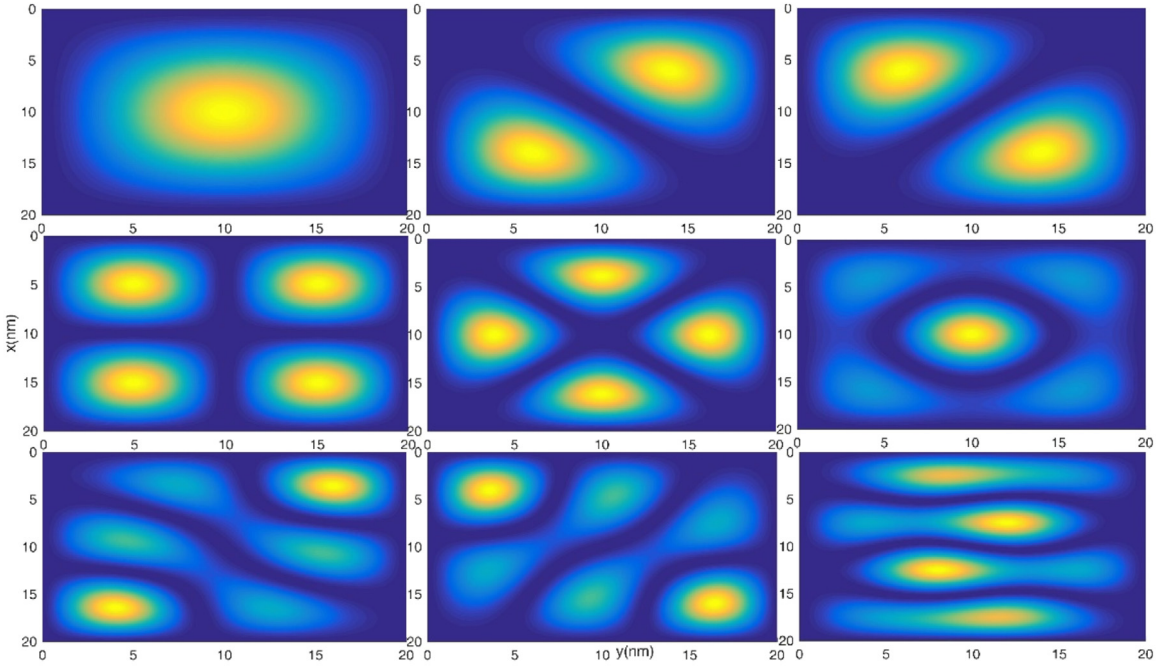

Fig. 1e. The probability densities of nine lowest eigenstates of a two-dimensional system with V(x, y)=0 as a function of the positions x (nm) and y (nm).

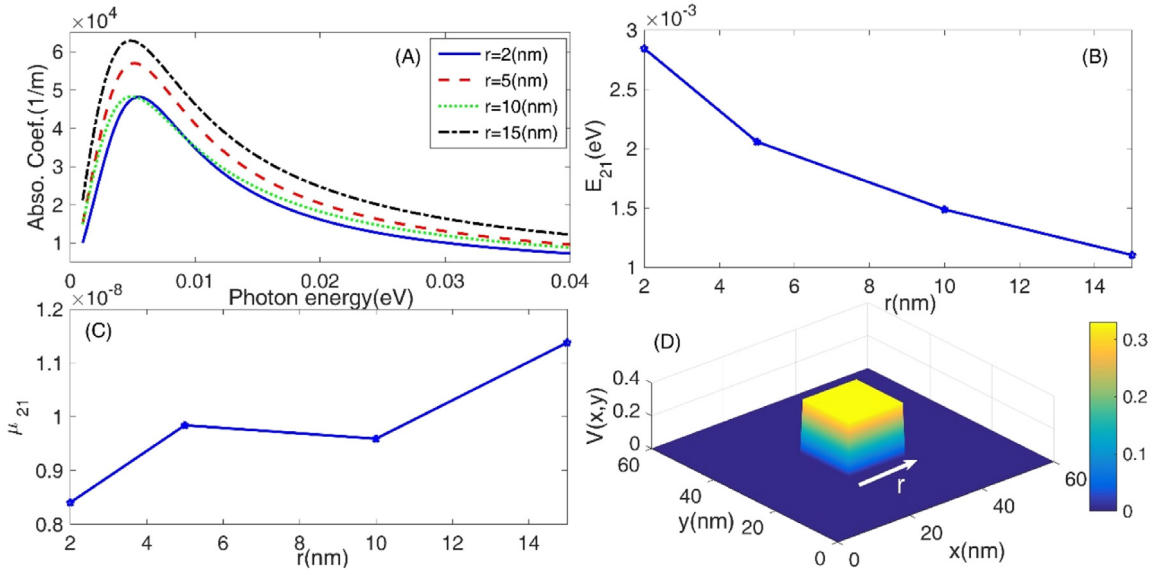

Fig. 2a. Panel (A): Variation of the absorption coefficient (1/m) as a function of the incident photon energy (eV). The effect of four different values of r (nm) has been shown in this panel. Panel (B): Variation of the transition energy E_{21} (eV) as a function of r (nm). Panel (C): Variation of the dipole matrix element μ_{21} as a function of r (nm). Panel (D): Variation of the case (I) Sierpinski carpet confining potential V(x, y) (eV) with iteration level 1 as a function of the x (nm) and y (nm).

3. Results and discussions

In our numerical calculations, we have used $GaAs/Al_xGa_{1-x}As$ Sierpinski triangles and Sierpinski carpets to compute the optical absorption coefficients of these two dimensional systems. Here, we fixed the total size of the system and changed the number of Sierpinski iterations and compared their optical absorption. We have also compared two cases I and II of confining potentials that are visible in the panels (I) of Figs. 1a and 1b, respectively. The case I and II Sierpinski systems actually are two special types of quantum dot and quantum Antidot lattices. To see an antidot potential in a square lattice see Ref. [64].

At first, we study the wave functions of a few fractal systems of the case I and II. Fig. 1a shows the probability densities of eight lowest eigenstates of a Sierpinski carpet of type (I) with Sierpinski iteration level 2 as a function of the positions x (nm) and y (nm). Panel (I) also shows the variation of the Sierpinski carpet confining potential V(x, y) (eV) as a function of the x (nm) and y (nm). As this figure shows, the maximum probability of finding electrons (yellow part in panel A to H) occurs in the well regions of the confining potential in the panel (I). Another fact is that by using the Sierpinski system we can manage the probability of finding the electron in any part of the system (i.e. wave function engineering). Fig. 1b is also the same as Fig. 1a but for case (II) confining potential. Figs. 1c and 1d are also the same as Figs. 1a and 1b, respectively, but for Sierpinski triangles. However, for comparison purposes, in Fig. 1e we have provided the nine lowest eigenstates of a two-dimensional system with V (x, y) =0. Comparing the case I and case II confining potentials reveals that in the case I potential, the wavefunctions are more distributed in the while parts of the system

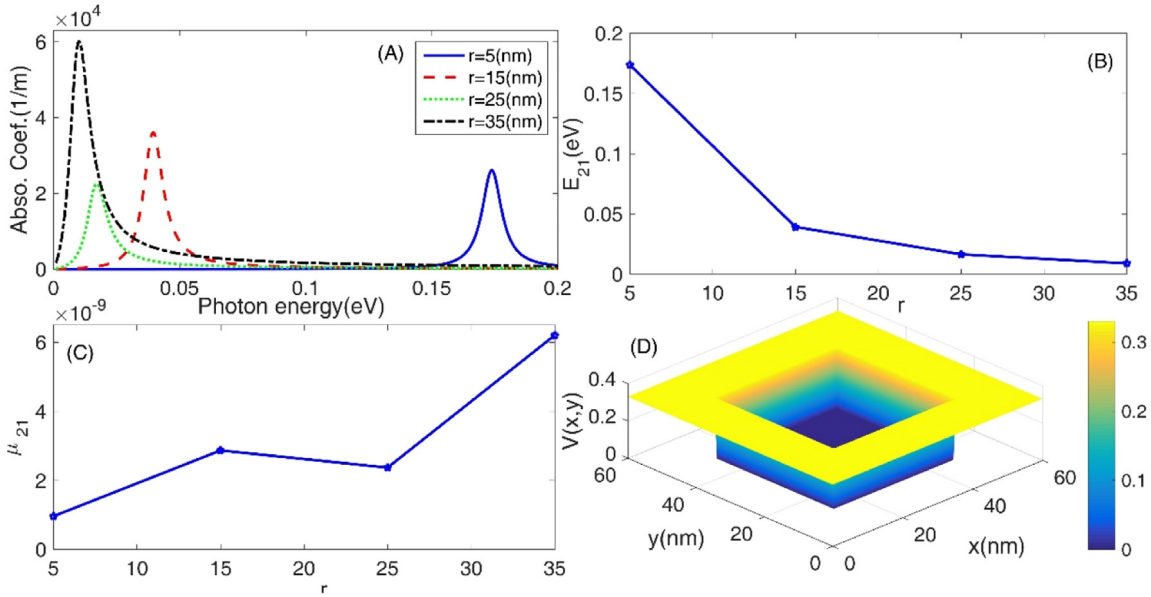

Fig. 2b. Same as Fig. 2a but for case (II) confining potential.

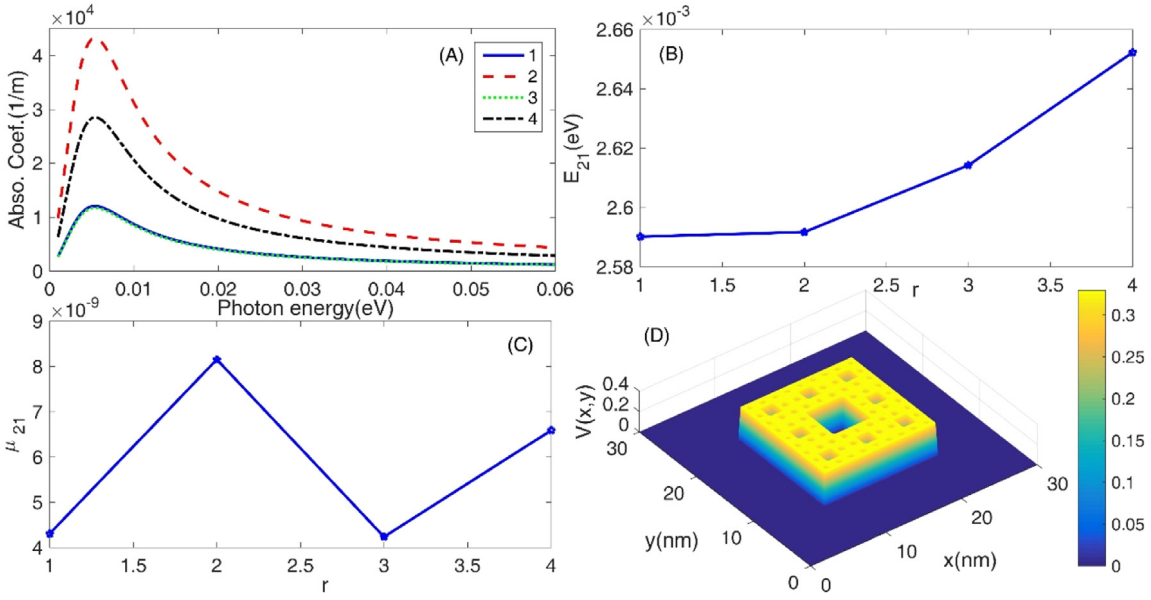

Fig. 3a. Panel (A): Variation of the absorption coefficient (1/m) as a function of the incident photon energy (eV). The effect of four different values of the Sierpinski iteration level has been shown in this panel. Panel (B): Variation of the transition energy E_{21} (eV) as a function of r (nm). Panel (C): Variation of the dipole matrix element μ_{21} as a function of r (nm). Panel (D): Variation of the case (I) Sierpinski carpet confining potential V(x, y) (eV) as a function of the x (nm) and y (nm) for Sierpinski iteration level 3.

and the case II ones, the wavefunctions are more localized in the central parts of the system. However, this is because, in the case I system, there is a large quantum well in the central part of the confining potential and in case II confining potential there is a large potential barrier in the central part on the system. The maximum probability of finding the electrons are located at the quantum wells. In the Sierpinski system, the barriers are fractally distributed in the system. Therefore by using the position of these barriers the shape and distribution of the wavefunction can be tuned. Comparing the Sierpinski systems with the clean system in Fig. 1e shows that the Sierpinski triangle confining potential breaks the wavefunction symmetry. However, the symmetry of the system is conserved when we add the Sierpinski carpet confining potential to the clean system. In Fig. 1e, we can see symmetry axes. For example in the panel E, the probability density are symmetric with respect to the diagonal lines of the panel square. This symmetry is present in the panel (E) of Figs. 1a and 1b but is absent in the panel (E) of Figs. 1c and 1d. Other symmetry axes, symmetry breaking and symmetry conservation can straightforwardly be identified in the panels of these figures.

Now, we discuss the optical absorption of the proposed Sierpinski systems. In the first step, in panel (A) of Fig. 2a, we have presented the variation of the absorption coefficient (1/m) as a function of the incident photon energy (eV). In this panel, the effect of four different values of r (nm) has been shown by four different lines. The parameter 'r' is shown in panel (D) of this figure. As this figure shows, the absorption peak position has not a monotonic behavior when we increased the length r. To describe this behavior, we have plotted the variation of the dipole matrix element μ21 as a function of r (nm) in the panel (C). As it is clear, the behavior of the absorption peak amplitude in the panel (A) is the same as the behavior of the dipole matrix element when r changes. However, the system with r=15 nm has maximum

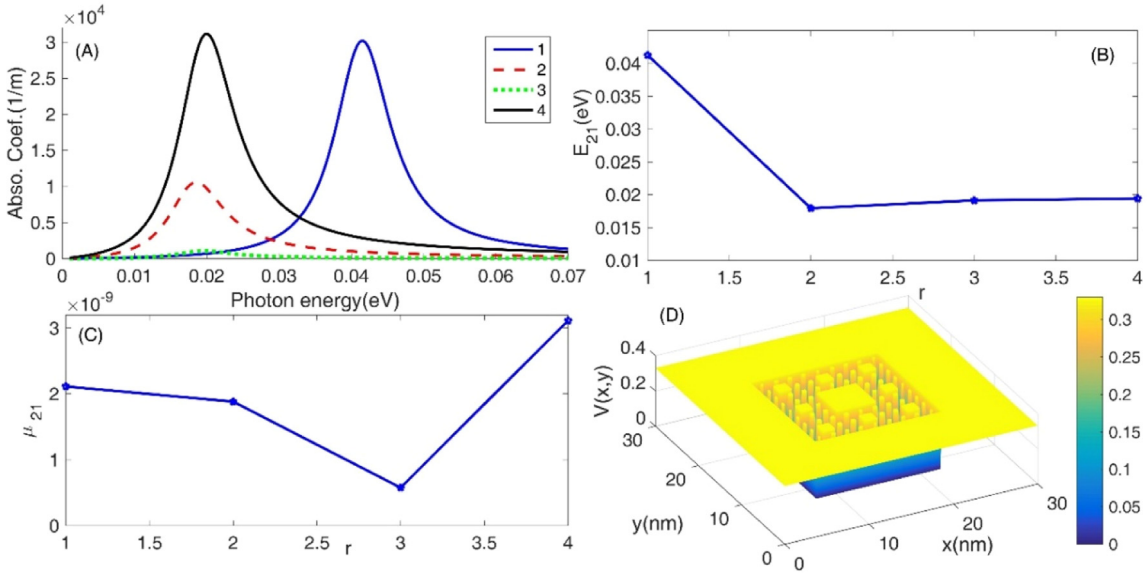

Fig. 3b. Same as Fig. 3a but for case (II) confining potential.

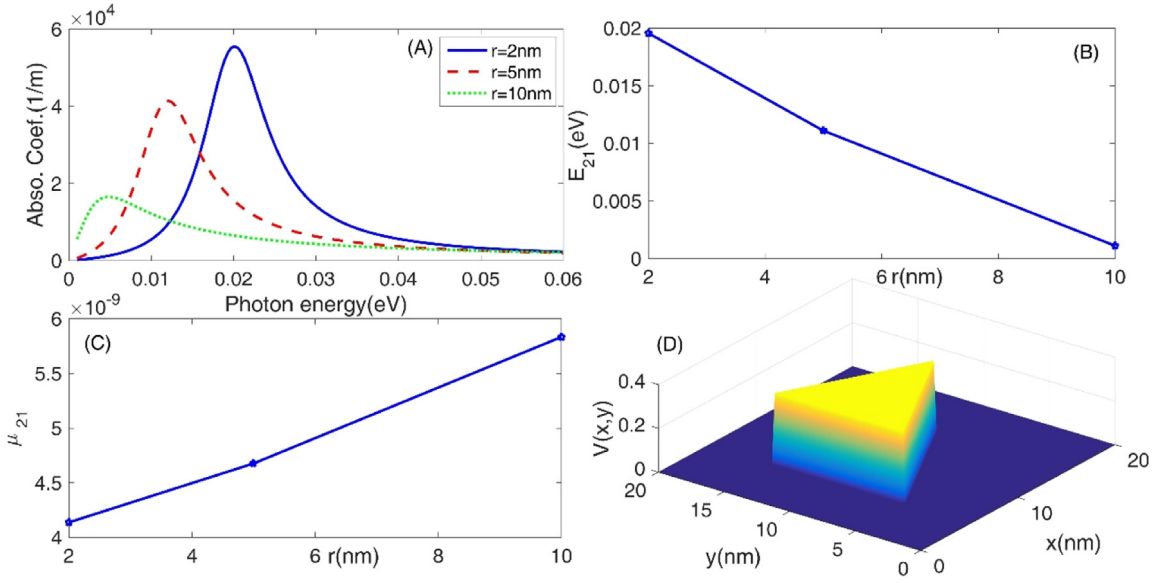

Fig. 4. Same as Fig. 2a but for a few Sierpinski triangles.

absorption amplitude among the studied systems. Besides, in the panel (B) we have plotted the variation of the transition energy E21 (eV) as a function of r (nm). This panel illustrates the variation of the absorption peak position as a function of the parameter r. as this panel shows, the absorption peak position moves toward lower energies (i.e. redshift) when r increases. Finally, in Panel (D) we have shown the variation of the case (I) Sierpinski carpet confining potential V(x, y) (eV) with iteration level 1 as a function of the x (nm) and y (nm) that we have studied in this figure. Fig. 2b is also the same as Fig. 1a but for case (II) confining potential. Comparing this figure with Fig. 2a reveals that the behavior of the absorption peak position and peak amplitude of the case I and II confining potential systems is the same. However, there is a difference. The effect of the parameter 'r' on the absorption peak position is greater in the case II confining potential system. This fact shows that the case II systems are more tunable than the case I ones.

In the next step, we study the effect of the Sierpinski iteration level on the absorption coefficient. In this way, we have plotted Fig. 3a. Panel (A) of this figure shows the variation of the absorption coefficient (1/m) as a function of the incident photon energy (eV). As this figure shows, the effect of the iteration level on the absorption peak amplitude is a decreasing oscillatory function. This behavior is visible in the panel (C) of this figure that shows the variation of the dipole matrix element μ21 as a function of r (nm). However, the absorption peak positions move toward higher energies (i.e. blueshift) when the Sierpinski iteration level increases. This behavior can be explained by using the variation of the transition energy E21 (eV) as a function of r (nm) that we have shown in the panel (B). However, for more illustration purposes, we have plotted the case (I) Sierpinski carpet confining potential V(x, y) (eV) as a function of the x (nm) and y (nm) for Sierpinski iteration level 3 in the panel (D). Fig. 3b is the same as Fig. 2a but for case (II) confining potential. Comparing this figure with Fig. 2a shows that, the effect of the Sierpinski iteration level on the absorption peak position and amplitude in the case I and II systems are different. In the case II model, the absorption peak positions move toward lower energies (i.e. redshift) when the Sierpinski iteration level increases. This behavior is in agreement with the variation of the transition energy

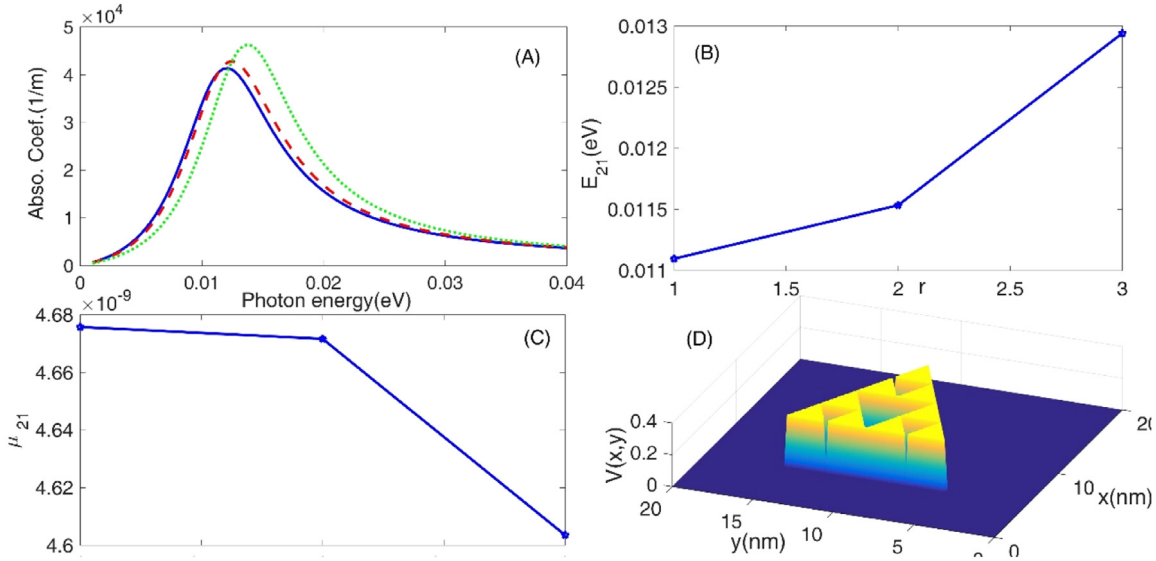

Fig. 5. Same as Fig. 3a but for a few Sierpinski triangles.

E21 (eV) as a function of r (nm) that we have shown in the panel (B). Besides, comparing the panels (A) of Figs. 2a and 2b shows that the case II systems are more tunable than the case I ones because a wider range of absorption amplitude can be obtained in the case II systems.

Now, we study the Sierpinski triangle and for this purpose, we have depicted the Fig. 4. Panel (A) of this figure shows the variation of the absorption coefficient (1/m) as a function of the incident photon energy (eV). The effect of four different values of r (nm) has been shown in this panel. Comparing these panels with the panel (A) of Fig. 2a shows that the behavior of the Sierpinski triangles is completely different from that of Sierpinski carpets. In this case, the Sierpinski triangle systems are more tunable than the Sierpinski carpet systems. In Fig. 4, when the parameter 'r' increases the absorption peak amplitude monotonically increases. This behavior is in agreement with the behavior of the dipole matrix element μ21 as a function of the parameter 'r' in the panel (C). The absorption peak position also monotonically moves toward the lower energies (i.e. redshift). This behavior is in agreement with the variation of the transition energy E21 (eV) as a function of r (nm) in the panel (B). For more illustrations, we have also plotted the variation of the case (I) Sierpinski triangle confining potential V(x, y) (eV) with iteration level 1 as a function of the x (nm) and y (nm) in the panel (D). Finally, we study the effect of the Sierpinski iteration level on the optical properties of the Sierpinski triangle systems. For this purpose, we have plotted Fig. 5. This figure is the same as Fig. 3a but for a few Sierpinski triangles. As this figure shows, in this case, the absorption peak position and amplitude do not drastically change. Comparing this figure with Fig. 3a shows that, the effect of the Sierpinski iteration level on the absorption coefficient is greater in the Sierpinski carpets than the Sierpinski triangles.

4. Conclusion

In this work, we studied the optical absorption coefficients of Sierpinski triangles and Sierpinski carpets. We demonstrated that, by using the proposed Sierpinski systems, the probability of finding the electron in any part of the system can be managed. The Sierpinski triangle confining potential broke the wavefunction symmetry but the Sierpinski carpet confining potential retained the symmetry of the system unchanged. In the Sierpinski carpet systems, the absorption peak position redshifted when r increased. The case II carpet systems were more tunable than the case I ones but the behavior of the absorption peak position and amplitude of these systems was the same. When the Sierpinski carpet iteration level in the case I model increased, the absorption peak amplitude had a decreasing oscillatory behavior and the absorption peak positions blueshifted. In the Sierpinski triangles, when the parameter 'r' increased the absorption peak amplitude monotonically increased and the absorption peak position redshifted. The effect of the Sierpinski iteration level on the absorption coefficient was greater in the Sierpinski carpets than the Sierpinski triangles but the effect of the parameter 'r' on the absorption coefficient was greater in the Sierpinski triangles than the Sierpinski carpets.

Declaration of competing interest

The authors declare that they have no known competing financial interests or personal relationships that could have appeared to influence the work reported in this paper.

References

[1] H. Balasubramanian, Two Photon Luminescence from Quantum Dots using Broad and Narrowband Ultrafast Laser Pulses (M.Sc. thesis), Texas A & M University, 2007, p. 12.
[2] T.W. Berg, J. Mørk, Saturation and noise properties of quantum-dot optical amplifiers, IEEE J. Quant. Electron. 40 (2004) 1527.
[3] S. Hellström, Z.-H. Chen, Y. Fu, 1.M. Qiu, R. Soltanmoradi, Q. Wang, J.Y. Andersson, Increased photocurrent in quantum dot infrared photodetector by subwavelength hole array in metal thin film, Appl. Phys. Lett. 96 (2010) 231110.
[4] L.W. Ji, S.J. Young, C.H. Liua, W. Water, T.H. Meen, W.Y. Jywe, Nitride-based light-emitter and photodiode dual function devices with InGaN/GaN multiple quantum dot structures, J. Cryst. Growth 310 (2008) 2476–2479.
[5] C. Wang, F. Grillot, J. Even, Impacts of wetting layer and excited state on the modulation response of quantum-dot lasers, IEEE J. Quant. Electron. 48 (2012) 1144.
[6] T. Sugaya, S. Furue, H. Komaki, T. Amano, M. Mori, K. Komori, S. Niki, O. Numakami, Y. Okano, Highly stacked and well-aligned In0.4Ga0.6As quantum dot solar cells with In0.2Ga0.8As cap layer, Appl. Phys. Lett. 97 (2010) 183104.
[7] X. Ma, S. John, Optical pulse dynamics for quantum-dot logic operations in a photonic-crystal waveguide, Phys. Rev. A 84 (2011) 053848.
[8] G. Wang, K. Guo, Excitonic effects on the third-order nonlinear optical susceptibility in parabolic quantum dots, Physica B 315 (2002) 234–239.
[9] S. Baskoutas, E. Paspalakis, A.F. Terzis, Effects of excitons in nonlinear optical rectification in semiparabolic quantum dots, Phys. Rev. B 74 (2006) 153306.
[10] B. Bansal, A model for the temperature dependence of photoluminescence from self-assembled quantum dots, J. Appl. Phys. 100 (2006) 093107.
[11] B. Alén, J. Bosch, D. Granados, J. Martínez-Pastor, J.M. García, L. González, Oscillator strength reduction induced by external electric fields in self-assembled quantum dots and rings, Phys. Rev. B 75 (2007) 045319.
[12] S.Y. Wei, L.L. Wei, C.X. Xia, X. Zhao, Y. Wang, Exciton states and interband optical transitions in ZnO/MgZnO quantum dots, J. Lumin. 128 (2008) 1285–1290.

[13] S. Shao, K.-X. Guo, Z.-H. Zhang, N. Li, C. Peng, Studies on the second-harmonic generations in cubical quantum dots with applied electric field, Physica B 406 (2011) 393–396.

[14] S. Shao, K.-X. Guo, Z.-H. Zhang, N. Li, C. Peng, Third-harmonic generation in cylindrical quantum dots in a static magnetic field, Solid State Commun. 151 (2011) 289–292.

[15] M. Solaimani, Miniband formation in GaN/AlN constant-total-effective-radius multi-shell quantum dots, Chin. Phys. Lett. 32 (11) (2015) 117304.

[16] W. Xie, Laser radiation effects on optical absorptions and refractive index in a quantum dot, Opt. Commun. 283 (2010) 3703–3706.

[17] M. Solaimani, M. Ghalandari, L. Lavaei, Donor impurity effects on optical properties of GaN/AlN constant total effective radius multishell quantum dots, J. Opt. Soc. Amer. B 33 (2016) 420–425.

[18] J.-H. Yuan, J.-S. Huang, M. Yin, Q.-J. Zeng, J.-P. Zhang, The correlation energies and nonlinear optical absorptions of an exciton in a disc-like quantum dot, Opt. Commun. 283 (2010) 3529–3532.

[19] Z.-H. Zhang, K.-X. Guo, B. Chen, R.-Z. Wang, M.-Wu. Kang, S. Shao, Theoretical studies on the optical absorption coefficients and refractive index changes in parabolic quantum dots in the presence of electric and magnetic fields, Superlattices Microstruct. 47 (2010) 325–334.

[20] M. Solaimani, L. Lavaei, S.M.A. Aleomraninejad, Optical rectification coefficients of cylindrical quantum dots: Rashba spin–orbit interaction effects, J. Opt. Soc. Amer. B 34 (2017) 1989.

[21] J. Huang, Libin, Dipole-allowed optical absorption in a parabolic quantum dot with two electrons, Phys. Lett. A 372 (2008) 4323–4326.

[22] M. Solaimani, Intersubband optical properties of three electrons confined in multishell quantum dots: comparison of two semiconducting compounds, J. Comput. Electron. 17 (2018) 1135–1142.

[23] T.O. Cheche, M.C. Chang, S.H. Lin, Electron–phonon interaction in absorption and photoluminescence spectra of quantum dots, Chem. Phys. 309 (2005) 109–114.

[24] I. Erdogan, O. Akankan, H. Akbas, Simultaneous effects of temperature, hydrostatic pressure and electric field on the self-polarization and electric field polarization in a GaAs/Ga0.7Al0.3As spherical quantum dot with a donor impurity, Superlattices Microstruct. 59 (2013) 13–20.

[25] G. Jolley, I. McKerracher, L. Fu, H.H. Tan, C. Jagadish, The conduction band absorption spectrum of interdiffused InGaAs/GaAs quantum dot infrared photodetectors, J. Appl. Phys. 111 (2012) 123719.

[26] G. Wang, K. Guo, Interband optical absorptions in a parabolic quantum dot, Physica E 28 (2005) 14–21.

[27] W. Xie, Optical properties of an off-center hydrogenic impurity in a spherical quantum dot with Gaussian potential, Superlattices Microstruct. 48 (2010) 239–247.

[28] M.C. Onyeaju, J.O.A. Idiodi, A.N. Ikot, M. Solaimani, H. Hassanabadi, Linear and nonlinear optical properties in spherical quantum dots: Generalized Hulthén potential, Few-Body Syst. 57 (2016) 793–805.

[29] D.B. Hayrapetyan, E.M. Kazaryan, H. Kh. Tevosyan, Direct interband light absorption in the cylindrical quantum dot with modified Poschl-Teller potential, Physica E 46 (2012) 274–278.

[30] W. Xie, Optical absorptions of an exciton in a disc-like quantum dot under an electric field, Opt. Commun. 283 (2010) 1381–1385.

[31] M. Zuhair, Effect of capping layer of GaAlAs on the electronic and optical properties of GaAs spherical layer quantum dot, Physica E 47 (2013) 275–278.

[32] E.C. Niculescu, Interlevel transitions in core–shell nanodots with dielectric environment, Superlattices Microstruct. 51 (2012) 814–824.

[33] C.Y. Lin, Y.K. Ho, Photoionization cross sections of hydrogen impurities in spherical quantum dots using the finite-element discrete-variable representation, Phys. Rev. A 84 (2011) 023407.

[34] W. Xie, Biexciton states trapped by a quantum dot, Physica B 391 (2007) 274–279.

[35] A. Ozmen, Y. Yakar, B. Cakır, U. Atav, Computation of the oscillator strength and absorption coefficients for the intersubband transitions of the spherical quantum dot, Opt. Commun. 282 (2009) 3999–4004.

[36] A.J. Williamson, J.C. Grossman, R.Q. Hood, A. Puzder, G. Galli, Quantum Monte Carlo calculations of nanostructure optical gaps: Application to silicon quantum dots, Phys. Rev. Lett. 89 (2002) 196803.

[37] Q.-F. Sun, J. Wang, T.-H. Lin, Photon sidebands of the ground state and the excited state of a quantum dot: A nonequilibrium green-function approach, Phys. Rev. B 58 (1998) 13007.

[38] S. Abdi-Ben Nasrallah, A. Bouazra, A. Poncet, M. Said, Theoretical investigation of intersubband transition energies and oscillator strength in CdS/SiO2 quantum dots, Physica E 43 (2010) 146–150.

[39] D. Shechtman, I. Blech, D. Gratias, J.W. Cahn, Metallic phase with long-range orientational order and no translational symmetry, Phys. Rev. Lett. 53 (1984) 1951.

[40] A.V. Lavrinenko, S.V. Zhukovsky, K.S. Sandomirski, S.V. Gaponenko, Scaling properties of an optical cantor filter, Phys. Rev. E 65 (2002) 036621.

[41] X.B. Cai, X.F. Xuan, Optical harmonic generation in a fibonacci dielectric superlattice of LiNbO3, Opt. Commun. 240 (2004) 227–233.

[42] L. Moretti, I. Rea, L. Rotiroti, I. Rendina, G. Abbate, A. Marino, L. De Stefano, Photonic band gaps analysis of Thue–Morse multilayers made of porous silicon, Opt. Express 14 (2006) 6264–6272.

[43] P. Hawrylak, J.J. Quinn, Critical plasmons of a quasiperiodic semiconductor superlattice, Phys. Rev. Lett. 57 (1986) 380.

[44] N.-H. L.iu, W.-G. Feng, X. Wu, Bulk and surface magnetoplasmon modes of cantor-type superlattices, J. Phys.: Condens. Matter 5 (1993) 4623.

[45] M. Kohmoto, B. Sutherland, K. Iguchi, Localization of optics: Quasiperiodic media, Phys. Rev. Lett. 58 (1987) 2436.

[46] A. Suto, Singular continuous spectrum on a Cantor set of zero Lebesgue measure for the Fibonacci Hamiltonian, J. Stat. Phys. 56 (1989) 525.

[47] X.-B. Cai, X.-F. Xuan, Optical harmonic generation in a fibonacci dielectric superlattice of LiNbO, Opt. Commun. 240 (2004) 227–233.

[48] M. Amini, M. Soleimani, M.H. Ehsani, Electronic and optical properties of GaAs/AlGaAs Fibonacci ordered multiple quantum well systems, Superlattices Microstruct. 112 (2017) 680–687.

[49] E. Macia, Thermal conductivity of one-dimensional Fibonacci quasicrystals, Phys. Rev. B 61 (2000) 6645.

[50] P. Ma, Y. Liu, Inflation rules b structure and localization of electronic states in a two-dimensional Penrose lattice, Phys. Rev. B 39 (1989) 9904.

[51] X. Yang, Y. Liu, Splitting rules for spectra of two-dimensional Fibonacci quasilattices, Phys. Rev. B 56 (1997) 8054.

[52] Y. Liu, Z. Hou, P.M. Hui, W. Sritrakool, Electronic transport properties of Sierpinski lattices, Phys. Rev. B 60 (1999) 13444.

[53] E. van Veen, S. Yuan, M.I. Katsnelson, M. Polini, A. Tomadin, Quantum transport in Sierpinski carpets, Phys. Rev. B 93 (2016) 115428.

[54] E.L. da Rocha, C.R. da Cunha, The transition from fracton to phonon states in a Sierpinski triangle lattice, Chaos Solitons & Fractals 44 (2011) 241–247.

[55] A.A. Iliasov, M.I. Katsnelson, S. Yuan, Hall conductivity of a Sierpiński carpet, Phys. Rev. B 101 (2020) 045413.

[56] R. Rammal, G. Toulouse, Spectrum of the Schrödinger equation on a self-Similar structure, Phys. Rev. Lett. 49 (1982) 1194–1197.

[57] E. Domany, S. Alexander, D. Bensimon, L.P. Kadanoff, Solutions to the Schrodinger equation on some fractal lattices, Phys. Rev. B 28 (1983) 3110–3123.

[58] B. Zhang, Y.W. Lu, H.P. Song, X.L. Liu, S.Y. Yang, Q.S. Zhu, Z.G. Wang, Depolarization blueshift in intersubband transitions of triangular quantum wires, J. Appl. Phys. 106 (2009) 113712.

[59] S.-S. Li, K. Chang, J.-B. Xia, Effective-mass theory for hierarchical self-assembly of GaAs/AlxGa1-xAs quantum dots, Phys. Rev. B 71 (2005) 155301.

[60] Y. Pan, X.-Z. Gao, M.-Q. Cai, G.-L. Zhang, Y. Li, C. Tu, H.-T. Wang, Fractal vector optical fields, Opt. Lett. 41 (2016) 3161.

[61] X.-Z. Gao, Y. Pan, M.-D. Zhao, G.-L. Zhang, Y. Zhang, C. Tu, Y. Li, H.-T. Wang, Focusing behavior of the fractal vector optical fields designed by fractal lattice growth model, Opt. Express 26 (2018) 1597.

[62] M. Solaimani, S.M.A. Aleomraninejad, L. Lavaei, Optical properties of parabolic quantum wires in the presence of electron–electron interactions: An euler–Lagrange variational application, Optik 172 (2018) 353.

[63] M. Solaimani, S.M.A. Aleomraninejad, Optical properties of energy-dependent effective mass GaAs/$Ga_xIn_{1-x}As$ and GaAs/$Al_xGa_{1-x}As$ quantum well systems: A shooting method study, J. Electron. Mater. 48 (2019) 942–950.

[64] T. Ando, S. Uryu, Chaotic transport in antidot lattices, J. Electron. Mater. 29 (2000) 557–564.